MICROSTRUCTURE AND MECHANICAL PROPERTIES OF WELDED JOINTS OF TITANIUM ALLOY Ti60 AFTER LASER WELDING AND SUBSEQUENT HEAT TREATMENT

Youqiong Qin,[1, 2] Danfeng Zhang,[1] Wenxiang Jiang,[1] and Xi He[1]

The methods of scanning electron microscopy and x-ray diffractometry are used to study the microstructure and mechanical properties of welded joints from alloy Ti60 after laser welding and subsequent heat treatment (PWHT). It is shown that the microstructure of the welded joint consists of three zones, i.e., a fusion zone (FZ), a heat-affected zone (HAZ) and base metal (BM). The PWHT lowers considerably the hardness in the FZ and in the internal HAZ, which results in a more homogeneous hardness profile as compared to the post-welding condition. After the heat treatment, the ultimate strength of the welded joint is 980 MPa at room temperature and 728 MPa at 600°C, the elongation is 10.9% at room temperature and 18.3% at 600°C.

Key words: alloy Ti60, laser beam welding, post-welding heat treatment, microstructure, mechanical properties.

INTRODUCTION

Titanium alloys are used widely in the aerospace, automotive and nuclear power industries and in ship building due to their high strength-to-weight ratio, fatigue strength and corrosion resistance [1, 2].

However, the low service temperature of traditional titanium alloys limits their application. A pseudo-α-alloy of the Ti – Al – Sn – Zr – Mo – Si system may be used at a maximum temperature of 600°C. Well-known pseudo-α-alloys are IMI-834, Ti-1100, BT-36, T600 and T60 [3 – 6].

Complex parts and assemblies from titanium alloys are often manufactured by welding. However, the chemical activity of titanium, which reacts easily with oxygen, hydrogen and nitrogen, results in worsening of the mechanical properties of welded joints. It is assumed that titanium alloys are less weldable than the conventional structural materials due to their susceptibility to environmental damage. As a rule, welding is conducted in an atmosphere of a protective gas or in vacuum. Today, components from titanium alloys are joined by electron beam welding (EBW) [3, 7], laser beam welding (LBW) [2, 8] and gas tungsten arc welding (GTAW) [9, 10]. After the GTAW, the mechanical properties of the joint are satisfactory, but the fusion zone (FZ) is coarse-grained, the heat-affected zone (HAZ) is wide, and the ductility is reduced, which restricts application of this kind of welding. EBW and LBW are more advantageous than GTAW due to the higher energy density, higher welding speed, lower heat input, and narrower fusion and heat-affected zones [3, 7]. However, the cost of the process of electron beam welding is very high due to the expensive equipment and necessity for an evacuated environment. This makes laser beam welding a more promising technique for joining titanium alloys.

Some metallurgical problems arise in laser beam welding of conventional titanium alloys. For example, the total elongation of a laser-beam-welded joint of alloy Ti6242 is lower than the elongation of the base metal (BM) due to formation of brittle phases (a high volume fraction of acicular α'-martensite in the FZ) [8]. The presence of a rigid FZ after LBW of alloy Ti – 6Al – 4V reduces the elongation of the joints [11, 12]. The lowering of the elongation is a result of formation of brittle phases (acicular α'-martensite), precipitation of hard brittle particles or formation of hydrides in the welded joint. As a rule, the ductility of welded joints of titanium alloys is enhanced by post-welding heat treatment (PWHT) [8, 13]. It has been shown in [13] that the elongation at fail-

---

[1] School of Materials Engineering, Shanghai University of Engineering Science, Shanghai, China.

[2] Shanghai Collaborative Innovation Center of Laser Advanced Manufacturing Technology, Shanghai University of Engineering Science, Shanghai, China.
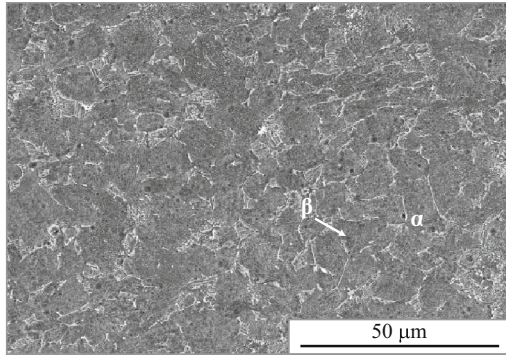
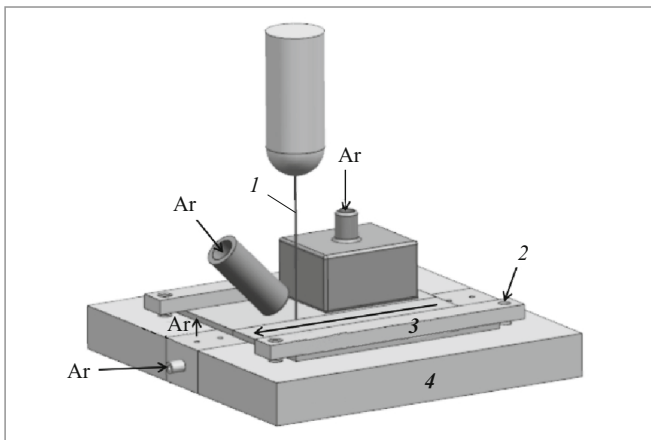**Fig. 1.** Microstructure of alloy Ti50 (base metal).

Fig. 3. Temperature diagram of PWHT.

Fig. 2. Scheme of the process of laser beam welding: *1*) laser beam; *2*) clamp, *3*) welding direction; *4*) sample support.

ure of a welded joint of alloy Ti – 6Al – 4V subjected to PWHT is 4 – 7%, which is lower than after the welding (14 – 15%).

Laser beam welding of traditional titanium alloys has been studied in many works, but the data on LBW of pseudo-α-titanium alloys with service temperature about 600°C, for example alloy T60, are scarce. The aim of the present work was to study the microstructure and mechanical properties of welded joints of titanium alloy T60 welded by the laser beam method. To improve the ductility of the joints we also resorted to PWHT.

METHODS OF STUDY

The base metal had the following nominal chemical composition (in wt.%): 5.7 Al, 3.8 Sn, 3.5 Zr, 0.89 Mo, 0.98 Ta, 0.39 Nb, 0.38 Si, the remainder Ti. This Ti60 pseudo-α-titanium alloy had a structure of fine equiaxed grains of α-phase with some β-phase over grain boundaries, as it is shown in Fig. 1. The temperature of the β-transformation of the alloy was 1050°C.

A sheet of alloy Ti60 was cut into samples $80 \times 40 \times 2$ mm in size. Before the welding, the surfaces of the sheet
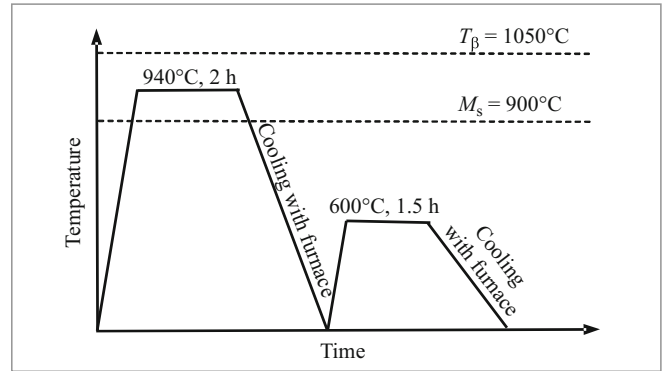
were cleaned from the oxide films by polishing with a SiC abrasive paper with grit 1000 and then treated with ultrasound in acetone. The welding was conducted with the help of a YLS-5000 fiber laser with maximum radiation power 5 kW. To protect the molten pool and the solidified fusion zone at high temperature from atmosphere, three kinds of protection with pure argon were applied, i.e., front shielding gas, back shielding gas, and protective cover gas with flow rates 25, 15, and 15 liters/min, respectively. Figure 2 presents the scheme of laser welding of alloy Ti60. The welding parameters were as a follows: laser power 2 kW, welding speed 1.2 m/min, defocusing 2 mm. After the welding, the joints were subjected to a heat treatment (PWHT) involving 2-h exposure at 940°C, cooling with the furnace to room temperature, 1.5-h exposure at 600°C, and cooling with the furnace to room temperature. The scheme of the PWHT is presented in Fig. 3.

We cut transverse metallographic specimens and specimens for tensile tests for each mode of welding and welding + PWHT. After grinding and polishing, the surface of the metallographic specimens was etched in Kroll's reagent (2 ml HF and 6 ml HNO_3 in 100 ml aqueous solution). The phase composition was determined with the help of an XPert PRO PANalytical x-ray diffractometer with copper K_α radiation at an accelerating voltage of 50 kV and a current of 200 mA. The microstructure and the fracture surfaces were studied using a scanning electron microscope (SEM) with an energy dispersive attachment for chemical analysis. The microhardness was measured at a load of 1 N (100 g) with a hold for 15 sec. The tensile tests were conducted at a speed of 2 mm/min at room temperature and at 600°C making at least three tests for each condition. The sizes and the shape of the specimens for the tensile tests are presented in Fig. 4.

RESULTS AND DISCUSSION

The appearance of the welding pool on the surface and in cross section of the weld are presented in Fig. 5. As a rule, the color of the top and bottom surfaces of a weld is determined by the efficiency of the gas protection from atmo-
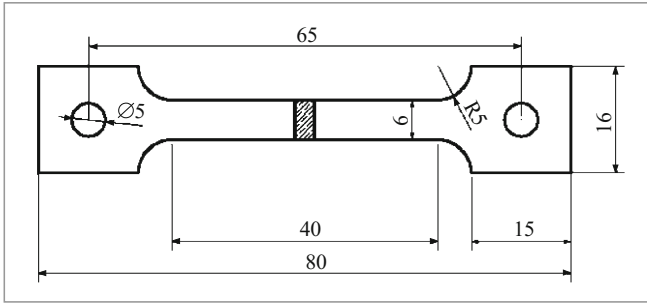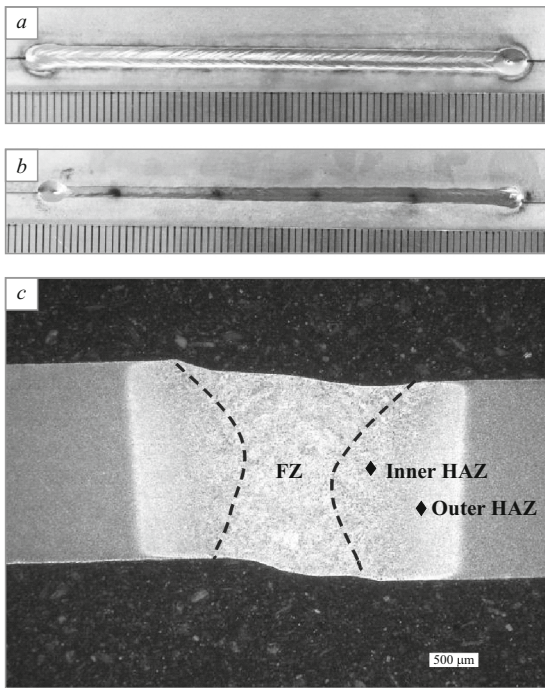
Fig. 4. Scheme of specimen for tensile testing.

Fig. 5. Appearance of welded joint and its cross section: *a*) upper surface of the joint; *b*) lower surface of the joint; *c*) cross section: FZ, inner HAZ, outer HAZ.

Fig. 6. Microstructure of the FZ (*a*) and of the HAZ (*b*, *c*) in the as-welded condition: *b*) inner HAZ; *c*) outer HAZ.

spheric contamination. The change in the color of the surface reflects the degree of the atmospheric contamination. It has been reported [14] that intensification of the contamination changes the color of the weld from a silver one to a light straw one and then to dark straw, dark blue, light blue, grey and, finally, powdery white colors. In our work the color of the top and bottom surfaces of the weld was silver and bright, which indicates a good gas protection of the welding pool from the atmospheric contaminations due to the three trajectories of the protective gas flows as it is shown in Fig. 5*a* and *b*.

Figure 5*c* shows full penetration of the liquid pool in the welded joint. The keyhole formation, the difference in the surface tensions, the considerable inhomogeneity of the recoil pressure over the depth of the keyhole, and the vortexes in the molten pool produce an X-shape weld. The welded
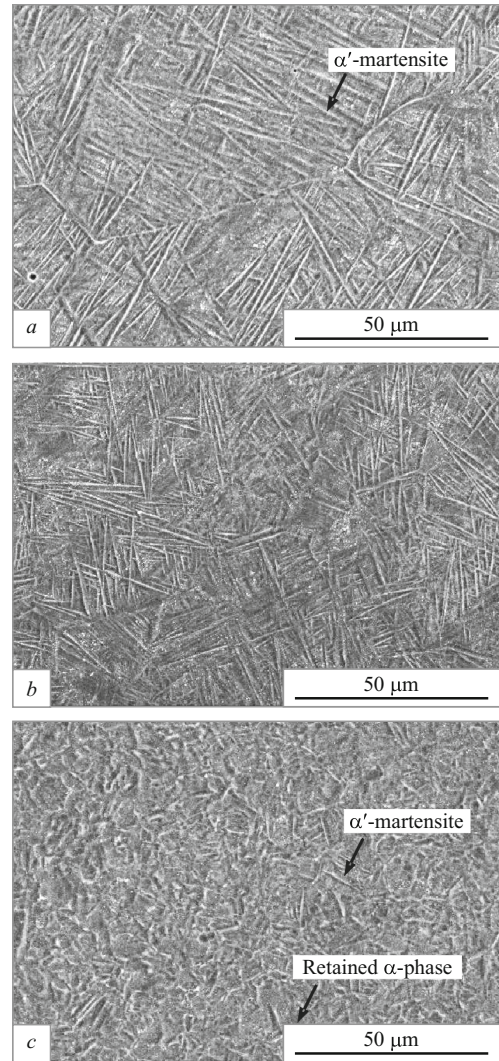
joint exhibits no crack or pore. The process of laser beam welding yields a high temperature gradient between the welding pool and the base metal, which causes formation of different zones, i.e., a fusion zone (FZ) and a heat-affected zone (HAZ) differing from the zone of the base metal (BM).

Figure 6*a* presents the microstructure of the FZ in the state after the welding. The microstructure of this zone consists of acicular α'-martensite. After the laser welding, the base metal cools and first transforms into a columnar β-phase. When the temperature of transformation of the β-phase is attained ($T_\beta = 1050°C$), the supersaturated β-phase cannot transform until the temperature of the start of martensitic transformation ($M_s = 900°C$), because the diffusion rate of the dissolved elements is not sufficient for nucleation and growth of α-phase in the β-matrix. In the course of the subsequent rapid cooling, the diffusion of the alloying elements and the decomposition of the solid solution are decelerated, and the β-phase with a bcc structure transforms
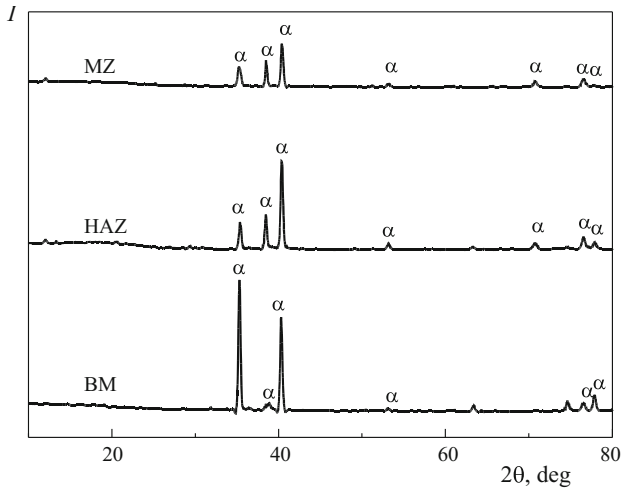
Fig. 7. X-ray diffraction patterns of as-welded specimens.

into α′-martensite with hexagonal close-packed (hcp) structure by a diffusion-free mechanism. The α′-martensite and the β-phase obey Burgers' relationship $(0001)_{\alpha'} // (011)_{\beta}$, $[11\overline{2}0]_{\alpha'} // [111]_{\beta}$ [15]. The results of the present work meet this relationship; the angle between the α′-martensite and the original β-phase is 30°, 60° and 90°. The width of the needles of the α′-martensite is $1 - 2$ μm.

Different regions in the HAZ (Fig. 6b and c) have undergone different thermal cycles and have accordingly different microstructures, i.e., an inner HAZ closest to the FZ and an outer HAZ closest to the BM as it is shown in Fig. 5c. In the inner HAZ, the temperature is higher than that of transforma-

tion of the β-phase (T_{β}) but lower than the melting point of the BM; the microstructure undergoes a complete martensitic transformation. The microstructure of the inner HAZ is represented by acicular α′-martensite similar to that observed in the FZ, but the size of the needles in it is smaller (Fig. 6b).

When the temperature of the HAZ is lower than that of transformation of the β-phase, the material is in a double-phase (α + β)-region. In the stage of heating, only a part of the α-phase transforms into β-phase, and the transformation in this zone in the stage of cooling is partial. Phase β transforms into acicular α′-martensite; phase α is preserved until room temperature (and is termed retained α-phase). The microstructure of the outer HAZ is mostly represented by acicular α′-martensite and retained α-phase (Fig. 6c). The content of the acicular α′-martensite decreases from almost 100% in the outer HAZ to almost zero with growth of the distance from the center of the welded joint to the outer HAZ.

The phase compositions of the FZ, the of HAZ and of the BM were determined with the help of x-ray diffractometry (Fig. 7). The diffraction peaks were indexed, and the picture proved that the structure was composed of a mixture of α/α′ phases. Reflections corresponding to β-phase were absent, because the content of the retained β-phase at room temperature was very low. However, it is very difficult to differentiate the α- and α′-phases because they have hcp structures with close lattice parameters.

Figure 8 presents the microstructure of the zones from the BM to the FZ after PWHT. Comparison with the struc-
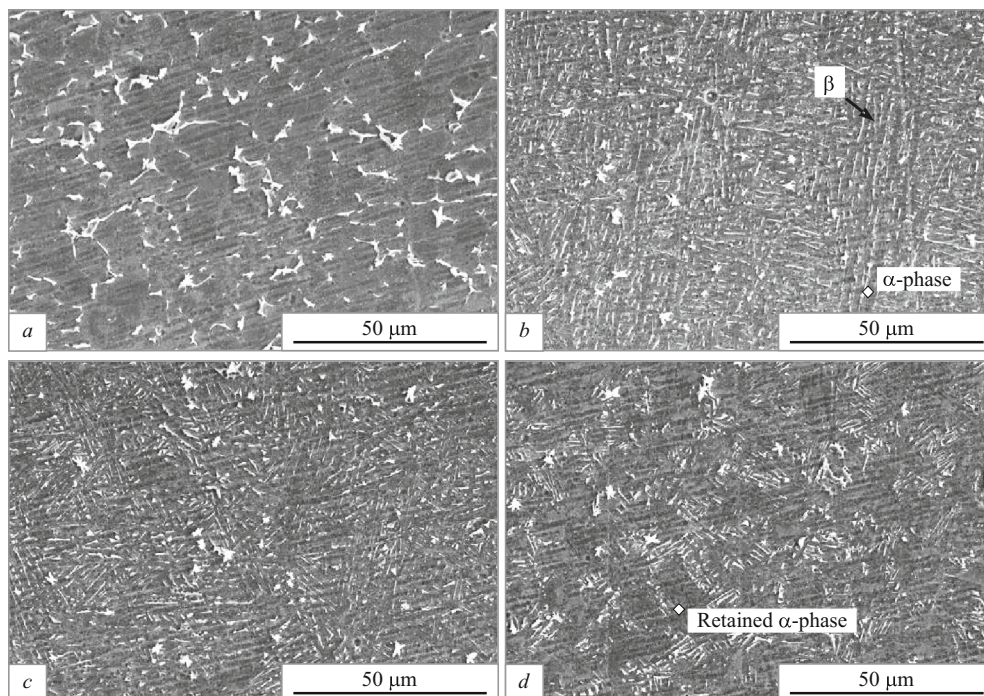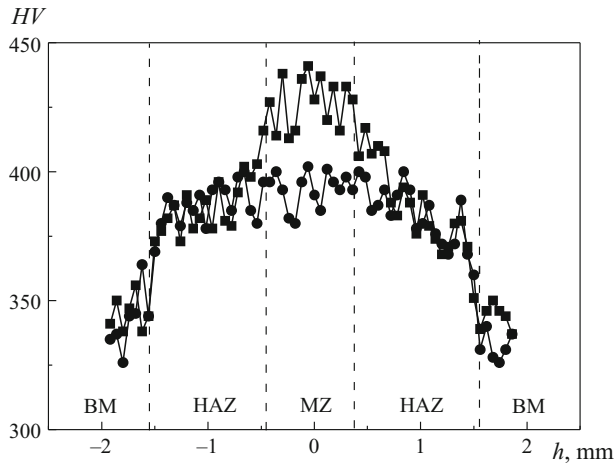

**Fig. 8.** Microstructure of welded joint after PWHT: *a*) base metal; *b*) FZ; *c*) inner HAZ; d) outer HAZ.

Fig. 9. Profiles of microhardness of welded joint after welding (■) and after PWHT (●) (*h* is the distance from the center of the weld).

Fig. 10. Localization of fracture in welded joints in different conditions: *a*) after welding at room temperature; *b*) after welding at 600°C; *c*) after PWHT at room temperature; *d*) after PWHT at 600°C.

ture of the BM in Fig. 1 shows that the type of the phases has not changed. The microstructure of the BM after the PWHT is chiefly represented by an equiaxed α-phase, but the grain size is larger (Fig. 8*a*).

Prior to the PWHT, the microstructure of the FZ is represented by acicular α'-martensite, which is a metastable phase. It can decompose after heating. During the PWHT, an α-phase will nucleate inside the fine acicular α'-martensite and some β-phase will precipitate between neighbor regions of the α-phase in the process of decomposition of α'-martensite. Since the α'-martensite and the original β-phase obey a Burgers orientation relationship, fine parallel particles of α-phase form in some cases (the black parallel regions of α-phase in Fig. 8*b*). Precipitation of β-phase restricts growth of the α-phase giving way to formation of a fine acicular α-phase surrounding a small content of β-phase.

The decomposition of the α'-martensite into a mixture of α- and β-phases is caused by redistribution of the dissolved atoms. This redistribution affects the evolution of the α/β interface and causes formation of grooves on the boundaries of the α-phase, where the β-phase has been located (the light phase in Fig. 8*b*). In accordance with this mechanism of the $\alpha' \rightarrow \alpha$ transformation in the $\alpha + \beta$ phase region, it has been shown in [16] that the yield strength and the elongation of titanium alloy Ti60 increase due to refinement of the α-phase. This is provided by annealing in the β-range and solution treatment in the $\alpha + \beta$ range; the annealing in the β-range yields α'-martensite, and a fine α-phase forms during the subsequent treatment in the $\alpha + \beta$ region.

Just like the FZ, the microstructure of the inner HAZ also contains a fine α-phase due to the smaller sizes of the original α'-martensite (Fig. 8*c*). The microstructure of the outer HAZ prior to the PWHT consists of α'-martensite and unchanged α-phase. During the PWHT, only the α'-martensite
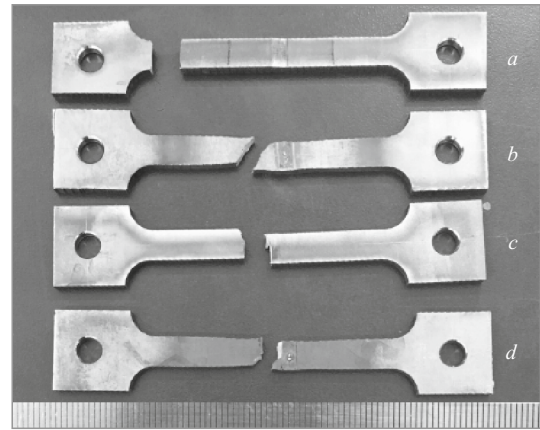
transforms into α-phase, and the α-phase remains invariable, i.e., the microstructure of the outer HAZ in the state after the PWHT is represented by acicular α-phase and retained α-phase.

Figure 9 presents the microhardness profiles over cross section of the welded joint after the welding and after the PWHT. After the welding, the microhardness is distributed nonuniformly. The microhardness in the fusion zone is very high (415 – 440 *HV*) and decreases gradually in the HAZ to the hardness of the base metal (340 *HV*).

Increase in the cooling rate results in formation of α'-martensite in the FZ and in the inner HAZ and yields accordingly high strength characteristics and reduced ductility. The content of α'-martensite attains almost 100%. The lowering of the hardness corresponds to a lower width of the α'-martensite needles in the inner HAZ as compared to the FZ. The content of the α'-martensite decreases gradually to about zero upon transition from the outer HAZ to the BM. The hardness decreases in accordance with the content of the α'-martensite in this region of the weld. Similar distribution of the hardness has been observed in [17] in laser welding of alloy Ti – 6Al – 4V.

As a result of the PWHT, the distribution of the hardness becomes almost uniform. The hardness in the FZ decreases to 380 – 400 *HV*. In the HAZ and in the BM the hardness decreases too.

The PWHT causes transformation of α'-martensite into a fine acicular α-phase, which lowers the hardness in the FZ and in the inner HAZ. Some lowering of the hardness is explainable by coarsening of grains.

Figure 10 presents the specimens for tensile tests. The location of fracture differs depending on the condition of the specimens. The properties of the BM and of the welded joints at room temperature and at 600°C are presented in Table 1. It can be seen that after the welding fracture develops
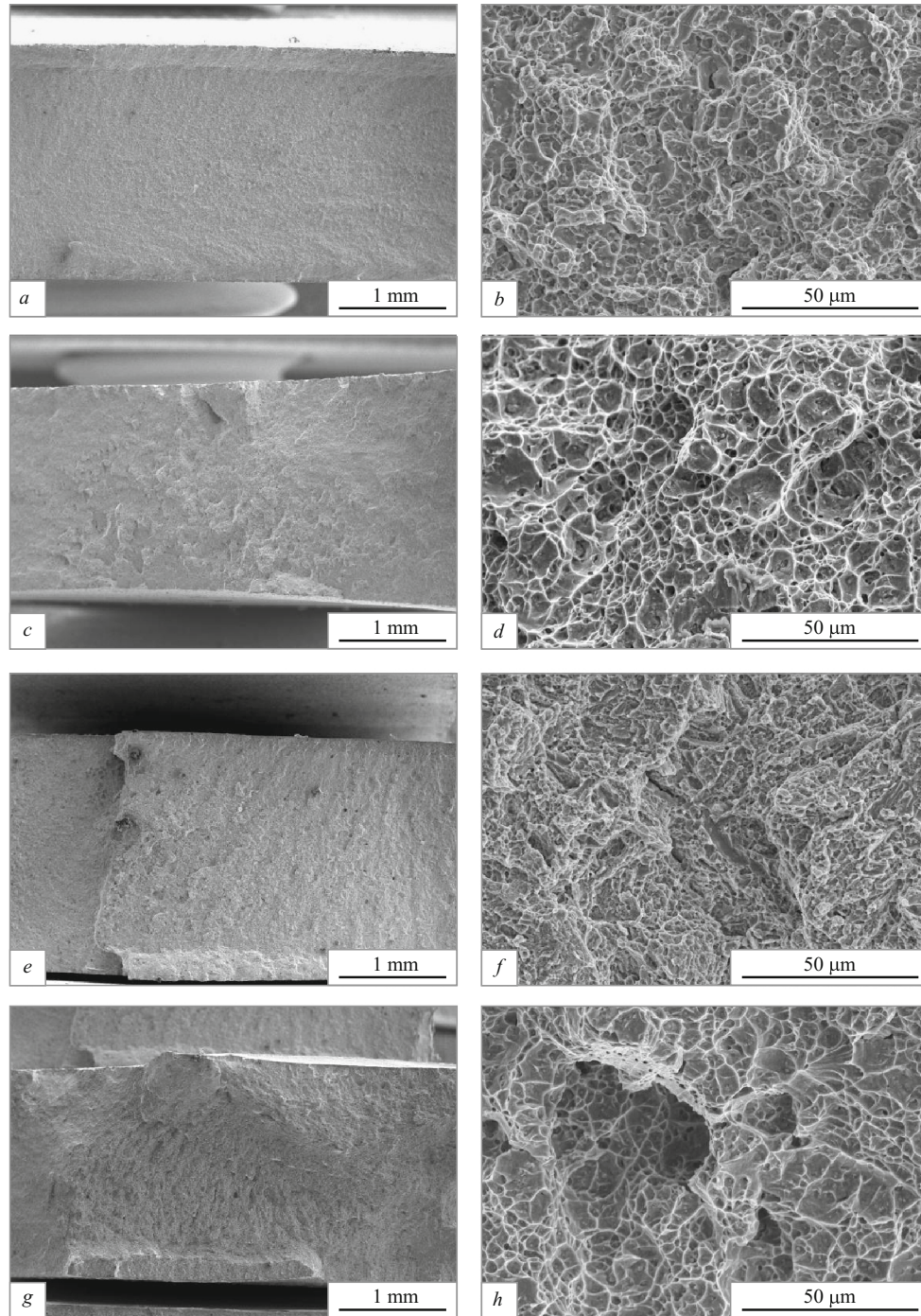
Fig. 11. Scanning electron microscopy of fracture surfaces of welded joints under low (*a*, *c*, *e*, *g*) and high (*b*, *d*, *f*, *h*) magnifications: *a*, *b*) after welding (T_{test} = 25°C); *c*, *d*) after welding (T_{test} = 600°C); *e*, *f*) after PWHT (T_{test} = 25°C); *g*, *h*) after PWHT (T_{test} = 600°C).

over the BM both at room temperature and at 600°C. The strength level is the same as that of the BM and the elongation of the welded joint is much lower than that of the BM. As a result of the PWHT fracture localizes in the FZ. The ultimate tensile strength after the PWHT is 87% of the BM at room temperature and 94% at 600°C. The PWHT raises the elongation with respect to the state as-welded, and it attains 10.9% and 18.3% at room temperature and at 600°C, respectively.

In the state after the welding, the growth of the strength and the lowering of the elongation are caused by formation of brittle α′-martensite in the FZ and in the HAZ. PWHT replaces the brittle α′-martensite by a more ductile α-phase causing a corresponding change in the properties.

TABLE 1. Properties of BM and of Welded Joints of Alloy Ti60 in Tensile Tests

Material	σ_r, MPa	δ, %	σ_r, MPa	δ, %	Localization of fracture
	$T_{\text{test}} = 25°C$		$T_{\text{test}} = 600°C$		
After welding	1191	9.2	771	12.2	BM
PWHT	980	10.9	728	18.3	FZ
BM	1130	12.6	745	14.0	–

Figure 11 presents the microstructure of fracture surfaces of welded joints at different magnifications. All the fracture surfaces contain dimples, which corresponds to a ductile fracture mechanism. The dimples are deeper after the tests at 600°C than after the tests at room temperature, which corresponds to the higher elongation at $T_{\text{test}} = 600°C$.

CONCLUSIONS

1. Laser welding of alloy Ti60 gives joints with a bright surface without contamination, cracks or porosity.

2. The structure of the fusion zone and of the inner heat-affected zone in the as-welded condition is represented by fine acicular α'-martensite. The outer HAZ consists of α'-martensite and untransformed retained α-phase. As a result of PWHT the α'-martensite transforms into a fine acicular α-phase.

3. In the state after welding, the profile of the hardness of the welded joint is nonuniform; the hardness is the highest in the center of the fusion zone ($415 - 440\ HV$). PWHT makes the distribution of the hardness more uniform, and its level decreases.

4. The as-welded joints fracture over the base metal; the ultimate strength amounts to 1191 MPa at room temperature and 771 MPa at 600°C; the elongation is 9.2 and 12.2%, respectively. After PWHT, the welded joints fracture in the fusion zone. The ultimate strength in this condition is 980 MPa at room temperature and 728 MPa at 600°C. The elongation is 10.9 and 18.2%, respectively. By the data of the fractographic analysis, the fracture mechanism is ductile.

REFERENCES

1. Yeganeh V. Esfahani and Peijie Li, "Effect of beam offset on microstructure and mechanical properties of dissimilar electron beam welded high temperature titanium alloys," *Mater. Design*, **124**(15), 78 – 86 (2017).

2. Kehuan Wang, Gang Liua, and Denis J. Politis, "Correlation between softening mechanisms and deformation non-uniformity of laser-welded alloy tube during gas bulging process," *Mater. Charact.*, **133**, 196 – 205 (2017).

3. G. Welsch, R. Boyer, and E. Collings, *Materials Properties Handbook: Titanium Alloys*, ASM Int. (1993).

4. J. Cai, M. Hao, X. Li, et al., "Study of composition character and microstructure of BT36 high temperature Ti alloy," *J. Mater. Eng.*, No. 2, 10 – 12 (2000).

5. J. Zhao, H. Ding, H. Hou, et al., "Influence of hydrogen content on hot deformation behavior and microstructural evolution of Ti600 alloy," *J. Alloys Compd.*, **491**(1), 673 – 678 (2010).

6. Z. B. Zhao, Q. J. Wang, J. R. Liu at al., "Effect of heat treatment on the crystallographic orientation evolution in a near-α titanium alloy Ti60," *Acta Mater.*, **131**, 305 – 314 (2017).

7. Chao Cheng, Bingbing Yu, Zhiyong Chen, et al., "Mechanical properties of electron beam welded dissimilar joints of TC17 and Ti60 alloys," *J. Mater. Sci. Technol.*, **34**(10), 1859 – 1866 (2018).

8. A. Chamanfar, T. Pasang, A. Ventura, et al., "Mechanical properties and microstructure of laser welded Ti – 6Al – 2Sn – 4Z – 2Mo (Ti6242) titanium alloy," *Mater. Sci. Eng. A*, **663**(29), 213 – 224 (2016).

9. A. Karpagaraj, N. Sivashanmugam, and K. Sankaranarayanasamy, "Some studies on mechanical properties and microstructural characterization of automated TIG welding of thin commercially pure titanium sheets," *Mater. Sci. Eng. A*, **640**(29), 180 – 189 (2015).

10. Guangsu Yan, Ming Jen Tan, Alexandru Crivoi, et al., "Improving the mechanical properties of TIG welding Ti – 6Al – 4V by post weld heat treatment," *Proc. Eng.*, **207**, 633 – 638 (2017).

11. A. Squillace, U. Prisco, S. Ciliberto, et al., "Effect of welding parameters on morphology and mechanical properties of Ti – 6Al – 4V laser beam welded butt joints," *J. Mater. Proc. Technol.*, **212**(2), 427 – 436 (2012).

12. E. Akman, A. Demir, T. Canel, et al., "Laser welding of Ti6Al4V titanium alloys," *J. Mater. Proc. Technol.*, **209**(8), 3705 – 3713 (2009).

13. Abu Syed H. Kabir, Xinjin Cao, Javad Gholipour, et al., "Effect of postweld heat treatment on microstructure, hardness, and tensile properties of laser-welded Ti – 6Al – 4V," *Metall. Mater. Trans. A*, **43**(11), 4171 – 4184 (2012).

14. G. Mathers, *Welding of Titanium and its Alloys, Pt. 1* (2016), p. 109.

15. R. Davis, H. M. Flower, and D. R. F. West, "Martensitic transformations in Ti – Mo alloys," *J. Mater. Sci.*, **14**(3), 712 – 722 (1979).

16. Feng Sun, Jinshan Li, Hongchao Kou, et al., "Effect of α′ martensite on microstructure refinement after α + β isothermal treatment in a near-α titanium alloy Ti60," *J. Mater. Eng. Perform.*, **24**, 1945 – 1952 (2015).

17. Chandan Kumar, Manas Das, and C. P. Paul, et al., "Comparison of bead shape, microstructure and mechanical properties of fiber laser beam welding of 2 mm thick plates of Ti – 6Al – 4V alloy," *Opt. Laser Technol.*, **105**, 306 – 321 (2018).